Gondwana Research 109 (2022) 416–428

Contents lists available at ScienceDirect

Gondwana Research

journal homepage: www.elsevier.com/locate/gr

Carbon isotope stratigraphy of Precambrian iron formations and possible significance for the early biological pump

H. Tsikos [a,*], M. Siahi [b,1], S. Rafuza [b], X.R. Mhlanga [b], P.B.H. Oonk [b,2], V. Papadopoulos [c], A.J. Boyce [c], P.R.D. Mason [d], C. Harris [e], D.R. Gröcke [f], T.W. Lyons [g]

[a] Department of Geology, University of Patras, GR-26504 Rio, Greece
[b] Geology Department, Rhodes University, Makhanda (Grahamstown) 6140, South Africa
[c] Scottish Universities Environmental Research Centre, East Kilbride G750QF, Scotland, UK
[d] Department of Earth Sciences, Utrecht University, Princetonlaan 8A, 3584CB Utrecht, the Netherlands
[e] Department of Geosciences, University of Cape Town, Rondebosch 7700, South Africa
[f] Department of Earth Sciences, University of Durham, South Road, Durham DH13LE, UK
[g] Department of Earth & Planetary Sciences, University of California, Riverside, CA 92521, USA

ARTICLE INFO

Article history:
Received 7 December 2021
Revised 17 April 2022
Accepted 12 May 2022
Available online 18 May 2022
Handling Editor: F. Pirajno

Keywords:
Iron Formation
Carbonates
Carbon isotopes
Stratigraphy
Biological pump

ABSTRACT

The origin of Precambrian iron-formations (IF) remains contentious, particularly with respect to the mineralogy of primary precipitates and the exact processes and conditions leading to their formation. Despite the uncertainties, prevailing hypotheses range from biological precipitation of ferrihydrite *to* abiotic water-column formation of greenalite. By contrast, iron carbonate minerals (siderite, ankerite) in IF have traditionally been attributed to diagenetic origins based on textural and isotopic relationships. Recent studies on IF from the Neoarchaean-Paleoproterozoic Transvaal Supergroup of South Africa have revealed evidence for apparently primary, low-$\delta^{13}C$, Fe/Mn-bearing Mg calcite as precursor to iron carbonate formation and as a potentially underestimated pathway of isotopically light carbon burial during IF deposition. Here, we present whole-rock $\delta^{13}C$ data and carbonate-specific geochemical analyses for samples from five drill cores that capture the entire stratigraphic extent of the Kuruman and Griquatown IF of the Transvaal Supergroup. Our results demonstrate remarkable consistency in stratigraphic profiles among the locations for the trends and magnitudes of bulk $\delta^{13}C$ values that are independent of paragenetic association, modal mineralogy, and chemical composition of the bulk carbonate fraction of each sample. We interpret these records as resulting from water-column abiotic carbonate formation that was accompanied by kinetic isotopic effects associated with fluctuating conditions (pH, alkalinity) controlling carbonate supersaturation in ambient seawater. Although our interpretation provides strong support for abiotic, anoxic models for IF genesis prior to the Great Oxidation Event (GOE), it does not entirely preclude additional biological mechanisms of primary ferric oxyhydroxide formation and its possible role in an early biological pump.

1. Introduction

Carbonate diagenesis in Precambrian (bio-)chemical sediments can limit the utility of carbon isotopes as a paleoceanographic proxy for the Earth's earliest oceans. In the specific case of iron-formations (IF), carbonate minerals are traditionally thought to have formed during early diagenesis through microbially mediated redox transformations within freshly precipitated sediment (Walker 1984; Nealson and Myers, 1990). Dissimilatory Iron Reduction (DIR) is assumed to be the predominant redox mechanism, in ways akin to modern anoxic diagenetic environments where sedimentary ferric oxyhydroxides are utilized by chemoautotrophic iron-reducing bacteria as terminal electron acceptors during anaerobic oxidation of co-occurring organic matter (Baur et al, 1985; Kaufman et al, 1990; Heimann et al, 2010; Johnson et al, 2013a). The net result is increasing DIC activity and dissolved Fe(II) concentrations in the pore fluids, which can stimulate iron carbonate precipitation. Today, DIR is only one part of a complex series of bacterially driven redox reactions utilizing several available electron acceptors during sediment burial (*e.g.*, Mn oxides,

* Corresponding author.
E-mail address: htsikos@upatras.gr (H. Tsikos).
[1] Presently at: Department of Geological Sciences, Missouri University of Science and Technology, Rolla, MO 65409, USA.
[2] Presently at: Nobian Salt B.V., Boortonweg 27, 7554RS Hengelo, the Netherlands.

https://doi.org/10.1016/j.gr.2022.05.007
1342-937X/

pore-water sulphate, etc.; Froelich et al, 1979). During the Precambrian, however, it is thought to have been the principal diagenetic process in the precursor sediment to IF because of large initial abundances of ferric species – postulated to have formed in a global ferruginous ocean – and contemporaneously low levels of dissolved sulphate (Crowe et al, 2014). Advocates for the importance of DIR during IF diagenesis cite as evidence the textural habit and low $\delta^{13}C$ values of the iron carbonate minerals, namely siderite and ankerite (Becker and Clayton 1972; Baur et al, 1985; Kaufman et al, 1990; Tsikos et al, 2003; Heimann et al, 2010; Johnson et al, 2013b].

Recent work by the authors on the carbonate record of well-preserved IF from the Neoarchean-Paleoproterozoic Transvaal Supergroup in South Africa, has highlighted the potential importance of primary carbonate precipitation in the form of low-$\delta^{13}C$, Fe/Mn-bearing Mg calcite, as apparent precursor for isotopically conservative siderite and ankerite formation (Siahi et al, 2020). The observed relationships and compositional signatures have led us to hypothesize that the low $\delta^{13}C$ record of the carbonate mineral fraction of IF may have been controlled mainly by water-column processes of carbon cycling and carbonate formation, rather than exclusively (or even dominantly) by microbially mediated diagenetic processes such as DIR.

In this study, we test the above hypothesis by focusing on new, stratigraphically controlled, whole-rock $\delta^{13}C_{carb}$ records across the entire IF sequence of the Transvaal Supergroup. Bulk-rock $\delta^{13}C_{carb}$ measurements were generated for the first time across several hundred meters of continuous IF stratigraphy captured in five drill cores located 10 s of km apart. Our data show a strikingly consistent stratigraphic pattern of $\delta^{13}C$ variation from the five locations expressed in both the trends and absolute values. We attempt to reconcile these observations both with prevailing theories for diagenetic carbonate mineral formation in IF *via* DIR, and with our alternative interpretation for primary carbonate formation. Recent studies on kinetic isotope fractionation effects during experimentally simulated growth of siderite in aqueous solutions (Jiang et al, 2022) allow us to critically question the DIR model for the origin of isotopically light carbonates and consider primary formation under temporally fluctuating conditions of carbonate saturation in the primary oceanic basin as an alternative. Our stratigraphically consistent records in bulk-carbonate $\delta^{13}C$ are therefore interpreted to reflect primarily variations in physicochemical parameters controlling carbonate (super)saturation in seawater through time – such as pH and seawater alkalinity – rather than strictly redox-related changes in the paleoenvironment of deposition. Although our interpretations and conclusions lend support mainly to abiotic models of IF deposition in an anoxic atmosphere–ocean system prior to the GOE, we cannot discount the possibility that biological mechanisms of primary iron oxidation may have contributed – at least partly – to IF genesis and to an active ancient biological pump, with ferric iron oxyhydroxide playing an additional key role as electron acceptor for organic carbon remineralization.

2. Geological background, materials and methods

The Kuruman and Griquatown IF of the 2.6–2.2 Ga Transvaal Supergroup [Beukes and Klein, 1990; Oonk et al, 2017; Siahi et al, 2020] together constitute one of the best preserved IF sequences of the Paleoproterozoic sedimentary record. The five drill cores selected for sampling (*i.e.,* GASESA, HEX, ERIN, AARPAN & LONDON) collectively capture the entire IF stratigraphy, which comprises the lower, microbanded Kuruman IF and the upper, granular to mesobanded Griquatown IF [Beukes and Klein, 1990; Oonk et al, 2017]. The drill cores were obtained by the local mining industry at localities with a maximum lateral separation in excess of 25 km in the geographical area northwest of Kuruman in the Northern Cape Province (Fig. 1). The total true stratigraphic thickness of the Transvaal IF succession in that area ranges approximately between 400 and 450 m, overlain and underlain, respectively, by glacial diamictite of the basal Makganyene Formation of the Postmasburg Group (Fig. 1) and carbonate rocks of the Campbellrand Subgroup.

All IF samples used here represent quartered-core sections across banding of lengths ranging between 5 and 10 cm. The bulk mineralogy is typical of IF and consistent across the entire stratigraphy and region, consisting of variable band-to-band combinations of micro-crystalline quartz, magnetite, carbonates (mixtures of siderite and ankerite with occasional calcite) and iron silicates (greenalite, minnesotaite, stilpnomelane and riebeckite). Hematite contents are practically undetectable in all our samples. The carbonate mineralogy, mineral chemistry and textural relationships have been comprehensively described by Siahi et al (2020). The selected samples therefore constitute mixtures of successive mm- to cm-scale bands, each with its own modal mineralogical identity.

The GASESA drill core, which extends into the underlying Campbellrand carbonates, is the only section that captures most of the Transvaal IF stratigraphy. The only gap is the uppermost *circa* 60 m of the Griquatown IF, which was percussion-drilled. In this core, an approximately 370 m interval of IF was sampled at low stratigraphic resolution — one sample per 15 m on average — for $\delta^{13}C$ analyses of bulk carbonate and organic carbon. The ERIN drill core, which captures the upper 275 m of the same IF stratigraphy, was sampled at a higher resolution of one sample approximately every 4–5 m. High resolution sampling, in addition to facilitating correlation with published data where possible, better captures the first-order carbonate-carbon isotope trends as well as the full range of bulk carbonate $\delta^{13}C$ and its finer-scale variation across stratigraphy. Stratigraphic profiles for bulk $\delta^{13}C_{carb}$ from the other three drill cores (*i.e.,* LONDON, HEX and AARPAN) capturing the upper 180–290 m of the Transvaal IF were generated at a resolution of one sample every 7–10 m on average, to compare the bulk carbonate-carbon isotope stratigraphy on a regional scale.

For bulk organic carbon and corresponding $\delta^{13}C$ analyses of drill core GASESA, bulk powdered samples were decalcified using 3 M HCl (at room temperature) in 50 ml centrifuge tubes for 16 h. Samples were subsequently neutralised with de-ionised water and dried at 40C for 36 h. The sample pellet was then reground and weighed into tin capsules for isotopic analysis. Stable isotope measurements were performed at Durham University in the Stable Isotope Biogeochemistry Laboratory (SIBL) using a Costech elemental analyser (ESC4010) coupled to a Thermo Scientific Delta V Advantage isotope ratio mass spectrometer. Carbon isotope ratios are corrected for ^{17}O and reported in the standard delta (δ) notation in per mil (‰) relative to Vienna Pee Dee Belemnite (VPDB). Isotopic accuracy was monitored through routine analyses of in-house standards and international standards (*e.g.,* IAEA-600, IAEA-CH-3, IAEA-CH-6, NBS 19, USGS24, USGS40). International and in-house standards are run daily and provided a linear range of $\delta^{13}C$ values between −46 ‰ and + 3 ‰ for isotopic correction. Analytical accuracy in $\delta^{13}C$ was better than 0.15 ‰ based on standards and replicate sample analysis. Total organic carbon data was obtained as part of the isotopic analysis using the internal standard glutamic acid (40.82 wt% C). Since TOC contents of the studied samples were very low, the sample size ranged between 80 and 100 mg of powder. The Costech elemental analyser was set to macro-oxygen for complete combustion to liberate all organic carbon. The isotope analyses were done in "no dilution mode," and all analyses produced a CO_2 signal greater than 800 mV, hence providing maximum confidence in the reported $\delta^{13}C$ values.

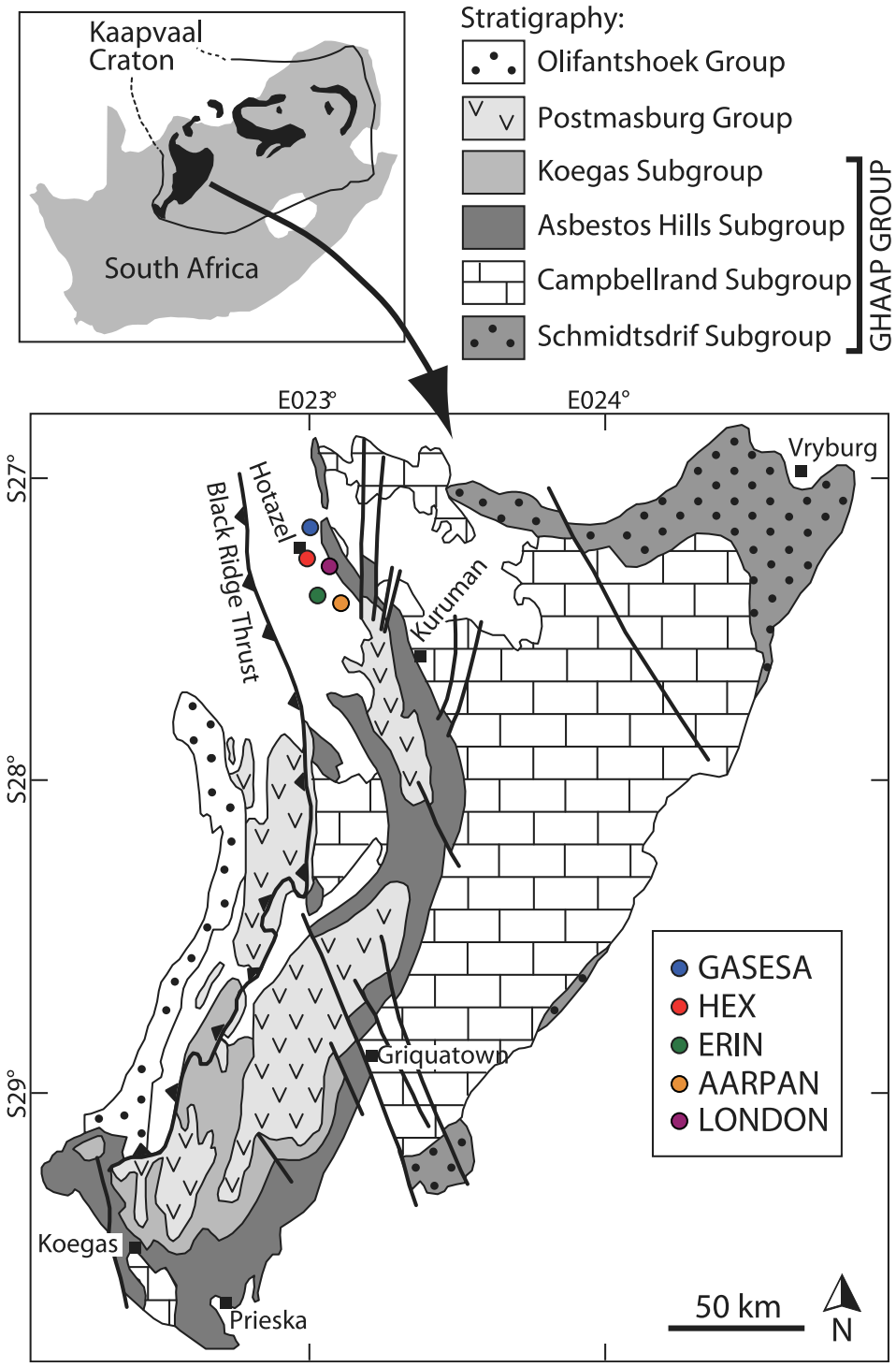

Fig. 1. Simplified regional geological map and stratigraphy of the Transvaal Supergroup (Griqualand West Basin) in the Northern Cape Province of South Africa. The localities of the five drill cores used in this study are shown NW of the city of Kuruman.

The carbonate-carbon isotope composition of samples from all drill cores was determined at SUERC on an Analytical Precision AP2003 mass spectrometer equipped with a separate acid injector system. CO_2 was released by reaction with 105 % H_3PO_4 under a helium atmosphere at 70 °C, after reacting for a minimum of seven days to ensure complete siderite dissolution. Carbon isotope ratios are reported relative to VPDB using the conventional delta (δ) notation. Mean analytical reproducibility based on replicates of the internal laboratory standard MAB-2 (Carrara Marble) was around ± 0.2 ‰. MAB-2 is extracted from the same Carrara Marble quarry as the IAEA-CO-1 international standard. It is calibrated against IAEA-CO-1 and NBS-19 and has the same C and O isotope values as IAEA-CO-1 (−2.5 ‰ and 2.4 ‰ VPDB, respectively).

Whole-rock $\delta^{13}C_{carb}$ isotope analyses for drill core ERIN were paired with determinations of major oxide abundances (CaO, FeO, MgO and MnO) of the bulk carbonate fraction based on the protocol of Poulton and Canfield (2005). Extractions were performed using 1 M sodium acetate [$C_2H_3NaO_2$] solution buffered

with acetic acid [CH_3COOH] to pH 4.5. For each sample, approximately 100–200 mg of bulk powder was placed in 15 ml centrifuge tubes, to which 10 ml of extraction reagent was added. The centrifuge tubes were placed on a shaker table for 48 h to ensure complete digestion of microcrystalline siderite. After extraction, the tubes were spun at 5000 rpm for 5 min, and a few ml of the extracts were decanted into polyethylene vials for chemical analysis.

Finally, six representative samples from drill core ERIN were also analysed sequentially for the $\delta^{13}C$ values of their ankerite and siderite fractions using the protocol of Al Aasm et al (1990), to assess possible mineral-specific isotopic controls on the corresponding bulk-rock $\delta^{13}C_{carb}$ values. Based on bulk carbonate content, between 10 and 50 mg of each sample powder were reacted in pure H_3PO_4 sequentially at 50 °C and 100 °C for 12 h (in water bath) and 1 h (in paraffin), respectively, at the stable isotope laboratory of the University of Cape Town. This methodology permitted extraction of $\delta^{13}C$ results that are specific to varyingly reactive carbonate fractions under the afore-mentioned temperatures, namely ankerite (along with minor calcite when present) at 50 °C and siderite at 100 °C. Like with the bulk-rock analyses, data for ankerite and siderite are reported against the VPDB standard using the standard δ notation.

3. Results

Carbon isotope and coupled elemental oxide results are presented in Tables 1 and 2 and displayed in Figs. 2 and 3. Fig. 2A is a low-resolution stratigraphic profile for drill core GASESA, which captures most of the Transvaal IF stratigraphy. The bulk $\delta^{13}C_{carb}$ record begins in the lower part of the Kuruman IF with values around −8 ‰, declining up section to just below −12 ‰ over the first 90 m of IF stratigraphy. This trend is followed by a small excursion to higher $\delta^{13}C_{carb}$ values, which fluctuate between −8.7 and −10.2 ‰ over the next 80 m of IF stratigraphy. A sharp positive excursion is recorded over the *circa* 60 m lithological transition between the Kuruman and Griquatown IFs, as the latter has been defined in previous studies (Beukes and Klein, 1990). Over that excursion, $\delta^{13}C_{carb}$ values range from −7.9 to −5.7 ‰. Bulk $\delta^{13}C_{carb}$ values then decline sharply within the lower portion of the Griquatown IF to minima between −13 and −11.2 ‰, with a broad trend of increasing $\delta^{13}C_{carb}$ recorded across the next 130 m of Griquatown IF stratigraphy.

For bulk organic carbon, $\delta^{13}C_{TOC}$ values of drill core GASESA average −28 ‰ across the entire section, ranging from values as high as −24 ‰ to as low as −33 ‰. No obvious correlation is observed with the corresponding bulk carbonate carbon isotope record (Fig. 2A). It should be noted, however, that the $\delta^{13}C_{TOC}$ values were derived from very low amounts of TOC in all samples — less than 0.1 wt% — and must therefore be interpreted with caution.

Fig. 2B shows the higher resolution bulk $\delta^{13}C_{carb}$ profile across the upper Kuruman and Griquatown IFs as captured in drill core ERIN. The diagram includes mineral-specific $\delta^{13}C$ analyses for six selected samples from the same profile to test whether variable modal carbonate mineralogy impacts the stratigraphic bulk $\delta^{13}C_{carb}$ signal. The data indicate that co-existing ankerite and siderite fractions co-vary with the corresponding bulk $\delta^{13}C_{carb}$ values within 1–2 ‰ of each-other, suggesting that mineralogical effects on bulk $\delta^{13}C_{carb}$ are minimal. Adjacent to the ERIN $\delta^{13}C_{carb}$ record,

Table 1
Carbon isotope data for drillcores GASESA (bulk carbonate and organic C) and drillcores HEX, LONDON and AARPAN (bulk carbonate only).

HEX		LONDON		AARPAN		GASESA		
Depth	$\delta^{13}C_{carb}$	Depth	$\delta^{13}C_{carb}$	Depth	$\delta^{13}C_{carb}$	Depth	$\delta^{13}C_{carb}$	$\delta^{13}C_{TOC}$
mbps	‰	*mbps*	‰	*mbps*	‰	*mbps*	‰	‰
−647.7	−8.4	−118.6	−7.9	−483.5	−6.4	−142.0	−9.5	−30.0
−651.5	−8.9	−127.8	−8.1	−490.2	−7.7	−149.5	−13.0	−33.5
−653.2	−6.4	−136.5	−7.5	−498.5	−7.9	−173.5	−11.2	−30.2
−656.1	−6.5	−142.1	−7.5	−508.5	−8.6	−191.5	−11.2	−26.8
−660.9	−7.1	−145.7	−6.5	−516.3	−9.2	−200.6	−11.4	−30.0
−667.0	−8.6	−151.1	−8.3	−527.0	−8.6	−212.0	−12.2	−26.6
−672.4	−8.1	−158.8	−8.2	−537.5	−8.9	−228.5	−12.9	−26.1
−685.4	−8.5	−167.6	−8.0	−542.0	−8.2	−244.0	−12.9	−27.4
−693.8	−7.6	−172.0	−12.3	−547.4	−9.2	−259.0	−11.7	−27.8
−705.8	−8.5	−178.6	−10.5	−559.9	−13.1	−265.5	−12.5	−26.6
−722.4	−9.2	−191.2	−11.0	−571.3	−12.1	−270.5	−7.1	−23.9
−733.4	−12.4	−197.7	−8.3	−578.0	−11.7	−282.5	−7.9	−30.3
−744.2	−10.9	−213.0	−9.9	−586.3	−10.1	−296.2	−6.7	−24.4
−752.8	−11.6	−224.6	−11.0	−596.0	−10.6	−336.4	−5.7	−27.0
−766.9	−11.2	−236.5	−10.8	−604.6	−10.6	−354.4	−9.3	−28.6
−780.1	−10.7	−249.5	−12.8	−614.2	−11.0	−366.5	−9.4	−28.4
−792.0	−11.3	−260.8	−13.1	−619.0	−10.6	−371.0	−10.2	−28.0
−802.4	−11.8	−271.7	−12.8	−629.3	−11.4	−389.5	−10.0	−31.8
−814.2	−12.6	−284.7	−7.3	−635.3	−12.2	−403.6	−9.9	−31.1
−827.4	−13.4	−288.9	−6.5	−648.5	−11.3	−419.5	−8.7	−26.2
−835.6	−12.3	−293.1	−8.9	−655.6	−10.4	−434.2	−12.3	−28.5
−848.9	−11.9	−296.5	−9.3	−660.9	−11.5	−441.0	−11.7	−27.4
−852.7	−9.7	−300.6	−10.3	−666.3	−6.6	−446.5	−11.6	−28.1
−858.9	−6.3	−303.2	−6.5	−670.4	−9.1	−460.5	−10.9	−27.1
−863.9	−8.3	−306.6	−7.2			−473.6	−9.2	−30.8
−867.5	−8.4	−307.0	−7.4			−488.4	−10.2	−27.2
−871.5	−8.9	−309.0	−7.8			−504.8	−9.5	−27.0
−886.5	−6.6	−320.9	−5.8			−512.9	−8.1	−26.1
−898.7	−9.8	−327.8	−8.4					
−919.8	−6.1	−332.9	−6.6					
−934.3	−5.9	−345.5	−6.0					
		−349.5	−6.4					
		−355.6	−8.1					

‰: per mil *vs* VPDB; *mbps*: meters below present surface.

Table 2
Carbon isotope data and carbonate-specific chemical analyses for drillcore ERIN.

Depth	$\delta^{13}C_{carb}$	$\delta^{13}C_{ank}$	$\delta^{13}C_{sid}$	MgO	CaO	MnO	FeO
mbps	*‰*	*‰*	*‰*	*wt%*	*wt%*	*wt%*	*wt%*
−376.5	−8.8			1.98	3.17	1.25	14.61
−381.9	−9.1			1.94	7.92	0.94	5.70
−383.6	−7.9			NA	NA	NA	NA
−384.2	−7.6			3.61	1.79	0.24	24.48
−386.7	−8.6			3.01	10.69	1.03	7.52
−388.6	−7.0			2.27	9.53	1.46	6.66
−390.2	−8.0			NA	NA	NA	NA
−394.6	−8.1			2.28	7.62	0.73	5.23
−396.5	−8.6			2.61	4.88	0.82	7.78
−399.2	−7.3			1.72	4.42	1.46	18.26
−405.2	−8.0	−8.6	−8.0	3.36	7.63	1.24	11.64
−405.6	−10.6			NA	NA	NA	NA
−407.6	−9.5			3.52	6.90	0.61	13.33
−424.0	−10.9			0.78	3.15	0.46	6.31
−430.8	−10.5			2.05	1.95	0.43	16.62
−432.3	−12.4			0.42	4.33	0.17	4.06
−436.4	−11.1			1.40	0.05	0.31	11.94
−449.8	−10.0			NA	NA	NA	NA
−455.3	−8.5			2.31	2.59	0.32	14.81
−461.4	−9.2			0.75	1.43	0.09	4.49
−464.6	−11.4			0.23	0.01	0.07	1.54
−467.6	−10.3	−10.4	−11.1	NA	NA	NA	NA
−468.2	−10.5			2.46	10.32	0.42	9.43
−473.3	−10.5			2.66	1.62	0.42	14.71
−476.4	−10.3			1.87	4.29	1.53	12.18
−478.3	−10.3			2.13	0.84	0.45	13.29
−481.6	−10.9			3.13	6.80	1.04	19.67
−488.8	−11.3			3.22	0.62	0.37	16.40
−495.4	−10.6			2.90	4.72	0.76	19.30
−498.8	−11.4			1.12	5.01	0.24	5.45
−509.8	−12.0			1.70	6.05	0.36	6.57
−512.5	−12.2			2.55	5.78	0.47	12.84
−515.3	−11.6			0.96	4.71	0.23	4.60
−518.4	−12.1			1.17	1.07	0.12	6.43
−520.5	−12.7			1.24	0.83	0.18	9.31
−523.8	−12.8	−11.7	−12.9	0.87	0.58	0.12	7.50
−525.9	−13.1			0.67	1.40	0.08	3.93
−528.3	−12.6			0.99	3.37	0.19	5.10
−535.3	−11.5			2.37	10.24	0.36	7.43
−538.1	−11.8			2.31	6.96	0.33	8.04
−543.4	−7.2			0.17	19.79	0.19	1.70
−546.3	−6.7			1.12	1.27	0.66	11.79
−550.4	−8.6			2.75	5.07	0.09	13.55
−555.3	−9.0	−7.9	−8.9	2.34	3.99	0.05	9.51
−557.4	−9.3			0.96	0.16	0.03	5.25
−561.6	−8.9			1.30	0.04	0.08	9.29
−565.3	−7.0			0.41	0.21	0.04	0.93
−571.9	−5.9	−5.6	−6.6	2.97	11.85	0.57	8.70
−575.4	−5.7			3.35	10.73	0.52	7.99
−578.2	−5.5			2.61	1.72	0.37	10.99
−579.4	−11.0			0.28	0.68	0.21	1.96
−586.8	−6.0			2.71	2.12	0.36	15.77
−593.6	−6.3			0.93	2.48	0.37	3.26
−595.3	−5.8			0.89	3.05	0.30	1.90
−604.5	−7.5			0.43	2.63	0.11	1.56
−608.3	−8.1			1.73	4.20	0.22	7.51
−609.5	−7.0			0.18	11.05	0.27	1.11
−618.4	−5.9			0.15	3.36	0.16	1.21
−627.5	−7.3			1.06	0.11	0.24	8.49
−637.3	−11.5			0.88	2.01	0.10	5.92
−643.1	−11.0			0.99	0.03	0.18	13.66
−645.7	−10.0	−8.5	−9.6	1.20	1.44	0.17	14.21

wt%: weight percent; *‰:* per mil *vs* VPDB; *mbps*: meters below present surface.

we plotted the corresponding profiles for carbonate-hosted CaO/FeO ratio and for modal carbonate (expressed as the wt% sum of all measured oxides) as determined through acetate extraction and subsequent chemical analyses. High variability in these two stratigraphic records (Fig. 2B) illustrates the correspondingly highly variable modal abundance and combined chemical composition of carbonate minerals (ankerite, siderite and/or calcite) across the examined drill core intersection. Isotopically, the overall high $\delta^{13}C_{carb}$ excursion plateau over the Kuruman-Griquatown IF transition is resolved into three distinct peaks and troughs of $\delta^{13}C_{carb}$ values that fluctuate by 2–3 ‰. This high $\delta^{13}C_{carb}$ plateau compares well with a published bulk carbonate-carbon isotope profile across the same part of the Transvaal stratigraphy (section "CORETSI" of Beukes and Klein, 1990; see also Fig. 2B).

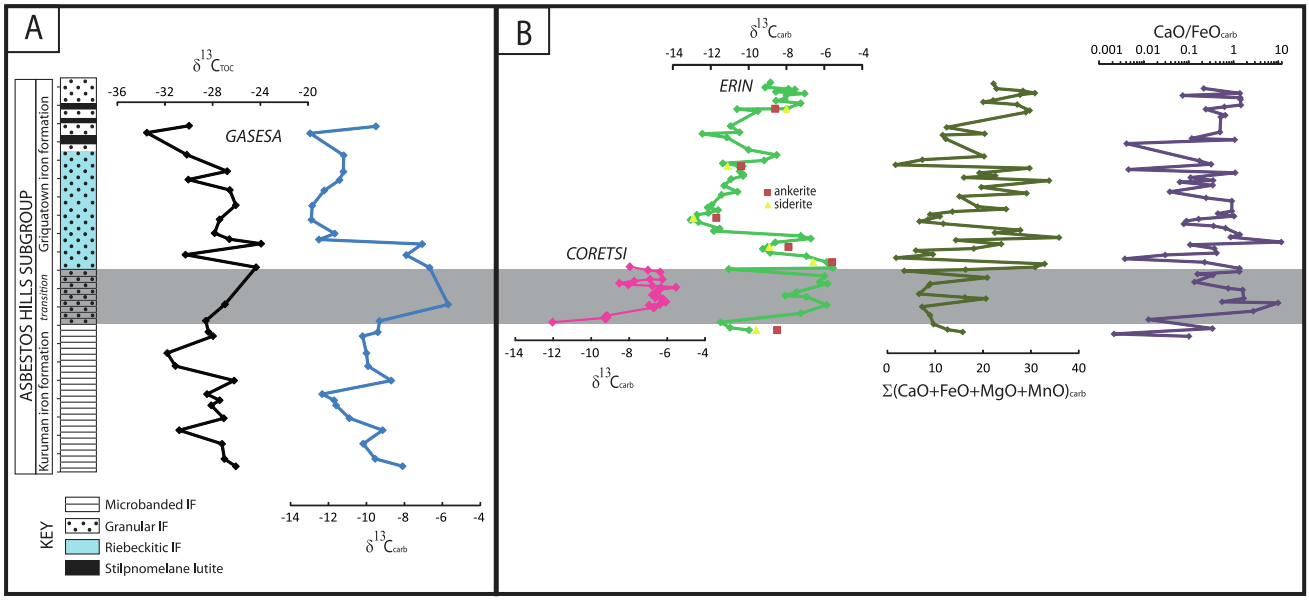

Fig. 2. A. Low-resolution carbon isotope stratigraphy for TOC and bulk-rock carbonate of drill core GASESA that intersects the largest part of the Asbestos Hills IF. B. High-resolution $\delta^{13}C$ record for bulk-rock carbonate from drill core ERIN that includes six samples analysed for their ankerite- and siderite-fraction $\delta^{13}C$. Corresponding stratigraphic records are also shown for bulk modal carbonate (expressed as the wt % total sum of carbonate-specific CaO, FeO, MgO and MnO data), and for the CaO/FeO ratio of the carbonate fraction for each sample. The CORETSI bulk-rock $\delta^{13}C_{carb}$ record displayed for comparison is sourced from Beukes and Klein (1990).

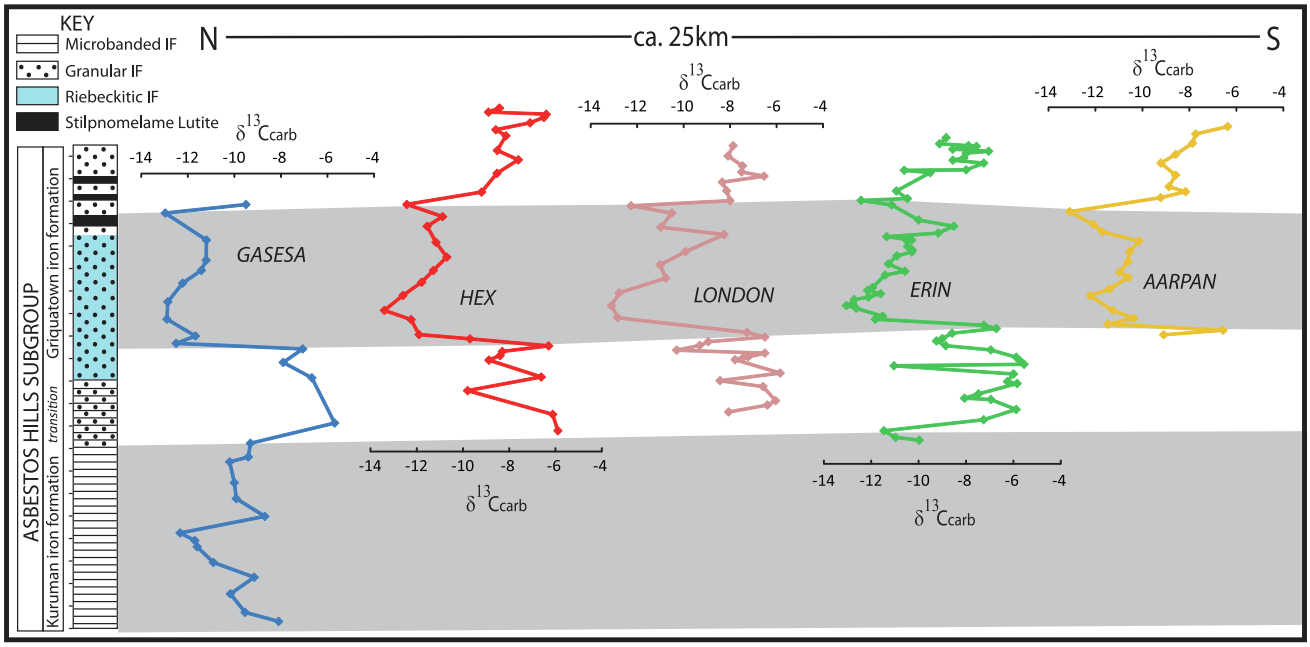

Fig. 3. Carbon isotope stratigraphy for the five drill cores used in this study, illustrating the regionally consistent pattern of stratigraphic variation in bulk-rock carbonate $\delta^{13}C$ values against the same depth scale below present surface. Variation in the thickness of individual segments of the carbon isotope curves from one drill core to another, are probably related to either primary lateral thickness variations and/or apparent thickness effects of variably dipping strata on the correspondingly vertical drill core intersections.

Up-section from the high $\delta^{13}C_{carb}$ plateau, data drop initially to a minimum of −13 ‰, and over the next 100 m of section increase gradually by 3–4 ‰ to values as high as −9 ‰ (Fig. 2B). Lithologically, this gradual positive $\delta^{13}C$ excursion develops within a riebeckite-rich subfacies at the lower part of the Griquatown IF [Beukes and Klein, 1990; Oonk et al, 2017]. A sharp negative $\delta^{13}C_{carb}$ spike to the value of −13 ‰ is recorded at the top of the latter excursion, superimposed on a broad transition between the lower riebeckite-rich facies and riebeckite-poor Griquatown IF above. Here, up to three characteristic stilpnomelane lutite layers are also observed consistently across all sampled sections (Oonk et al, 2017). Thereafter, $\delta^{13}C_{carb}$ values rise again to as high as −7 ‰ over the remaining 80 m of Griquatown IF stratigraphy. This pattern of stratigraphic bulk $\delta^{13}C_{carb}$ variation is faithfully recorded in the remaining three drill cores (*i.e.*, AARPAN, HEX and LONDON; Fig. 3).

4. Discussion

Important benchmarks for any discussion on the significance of the stratigraphic $\delta^{13}C_{carb}$ record of carbonate minerals in IF are the ranges and means that $\delta^{13}C_{carb}$ values attain in IF occurrences globally. To this end, we have compiled published $\delta^{13}C_{carb}$ data for different IF from the earliest Paleoproterozoic (as obtained mostly from bulk-rock analyses and much less so from mineral-specific ones) including our new data presented in this paper. We summarily present these data in the histograms of Fig. 4. Although the dataset displayed is dominated by IF of the Transvaal Supergroup and less so by those from the Hamersley Basin in Australia, two striking observations can be readily gleaned: the first is the consistent range of $\delta^{13}C_{carb}$ data between the values of −13 and −5 ‰ for more than 95% of the plotted global dataset; the second is the close similarity in the mean value of each subset displayed, which lies within a maximum of 0.7 ‰ from the global mean $\delta^{13}C_{carb}$ at −9.6 ‰.

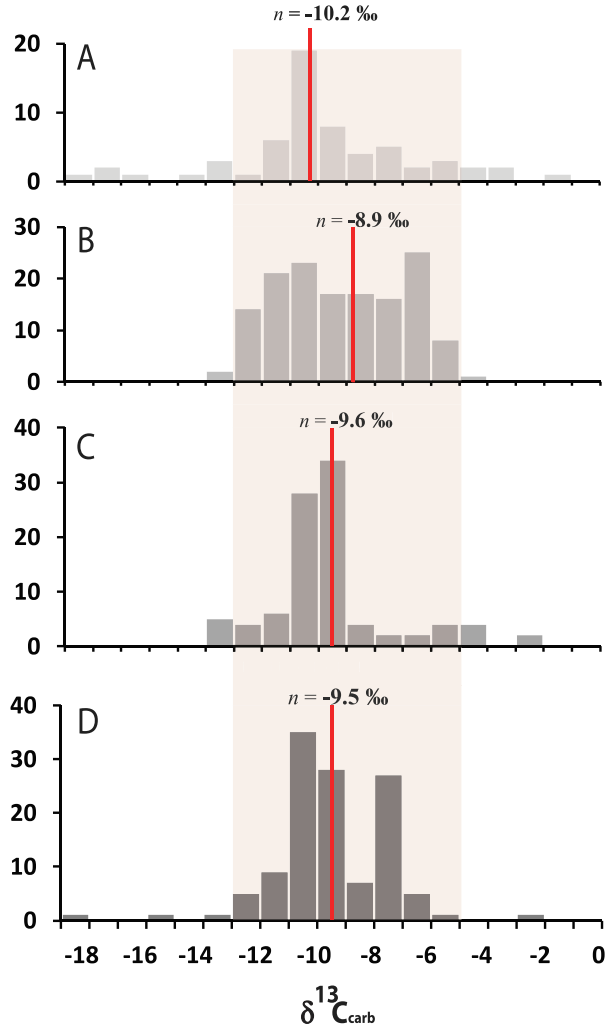

Fig. 4. Histograms displaying ranges of carbonate-carbon isotope data from various Archean-Paleoproterozoic IF around the globe. A. Hotazel Formation IF (Tsikos et al, 2003; Schneiderhahn *et al*, 2006; Mhlanga, 2019); B. Kuruman and Griquatown IF (Beukes and Klein 1990; this study); C. Koegas Subgroup IF (Johnson et al, 2013b); D. Hamersley IF (Becker and Clayton 1972; Baur et al, 1985; Kaufman et al, 1990). Note that all deposits plotted are of low metamorphic grade with maximum burial temperatures of ~ 300 °C for the Hamersley Basin, and ~ 150 °C for the Transvaal Basin (Klein and Gole, 1981; Miyano and Klein, 1983; Klein, 2005).

The second piece of background information that informs the nature and origin of carbonate minerals in IF is their textural habit and any related variability as observed across the IF occurrences studied. The backscattered electron images of Fig. 5 provide a snapshot of typical carbonate textures and intergrowths on various scales from the South African IF record (Siahi et al, 2020). The observed textures take the form of fine-grained populations of subhedral to almost perfectly rhombohedral ankerite and siderite grains, with the former usually attaining larger crystal sizes compared to co-existing siderite. These textures have been variously attributed in the literature to diagenetic carbonate (re-) crystallisation *sensu lato*, although in most instances there is no precursor species to iron carbonate formation identified. In the sections that follow, we attempt to elucidate further the origin of the carbon isotope signature of iron formation carbonates within the context of prevailing textural relationships and considering both previously published details and our new results and observations as presented in this paper.

4.1. Diagenetic controls on carbonate-carbon isotopes in IF

Classic interpretations of diagenetic iron carbonate formation *via* DIR have been presented in many previous publications (*e.g.*, Baur et al, 1985; Kaufman et al, 1990; Heimann et al, 2010) and were also comprehensively reviewed by Siahi et al (2020). Therefore, only a few salient aspects of the DIR model will be revisited here with relevance to the discussion that follows. In principle, DIR during anaerobic diagenesis implicates organic carbon oxidation and re-mineralisation by reaction with primary ferric precipitates. The latter are thought to have been dominated by primary ferrihydrite formed during photoferrotrophy, although we cannot exclude other inorganic or biological pathways of ferric oxyhydroxide formation. A standard chemical reaction that describes DIR is shown below:

$$CH_2O + 4Fe(OH)_3 \rightarrow FeCO_3 + 3Fe^{2+} + 6OH^- + 4H_2O$$

The above reaction suggests that iron carbonate formation will, in principle, progress until either of the two reactants – namely organic carbon or ferric oxyhydroxide – is exhausted. The presently observed mineralogy of IF, and specifically the abundance of ferric iron in magnetite and conspicuous lack of preserved organic carbon (Dodd et al, 2019; Thompson et al, 2019), point to the latter being the obvious limiting factor in iron carbonate generation during diagenesis.

Recent studies have attempted to address the dearth of organic carbon in IF (Dodd et al, 2019; Thompson et al, 2019; Jelavic et al, 2020), each from a somewhat different point of view. The study of Thompson et al (2019) holds special relevance to our current considerations: it specifically proposes that the bulk of biomass deposition would have been physically decoupled from ferric oxyhydroxide deposition during the formation of IF, in broad agreement with findings presented in other independent studies (*e.g.*, Jelavic et al, 2020). This decoupling would have resulted in the TOC-deficient nature of IF precursor sediment and the concomitant lateral migration and deposition of much of the primary biomass into coastal sediments, where it would have been converted into methane during diagenetic fermentation reactions. Methane delivery ultimately into the early atmosphere would have potentially played a major role as climate modulator under a dim young sun (Thompson et al, 2019).

The model by Thompson et al (2019) summarized above bears direct significance on the interpretation of the $\delta^{13}C_{carb}$ record of IF, as it implies that the typical range of $\delta^{13}C_{carb}$ values in IF carbonate minerals as shown in Fig. 4 would reflect mixing of two marine carbon reservoirs with correspondingly contrasting $\delta^{13}C$ values,

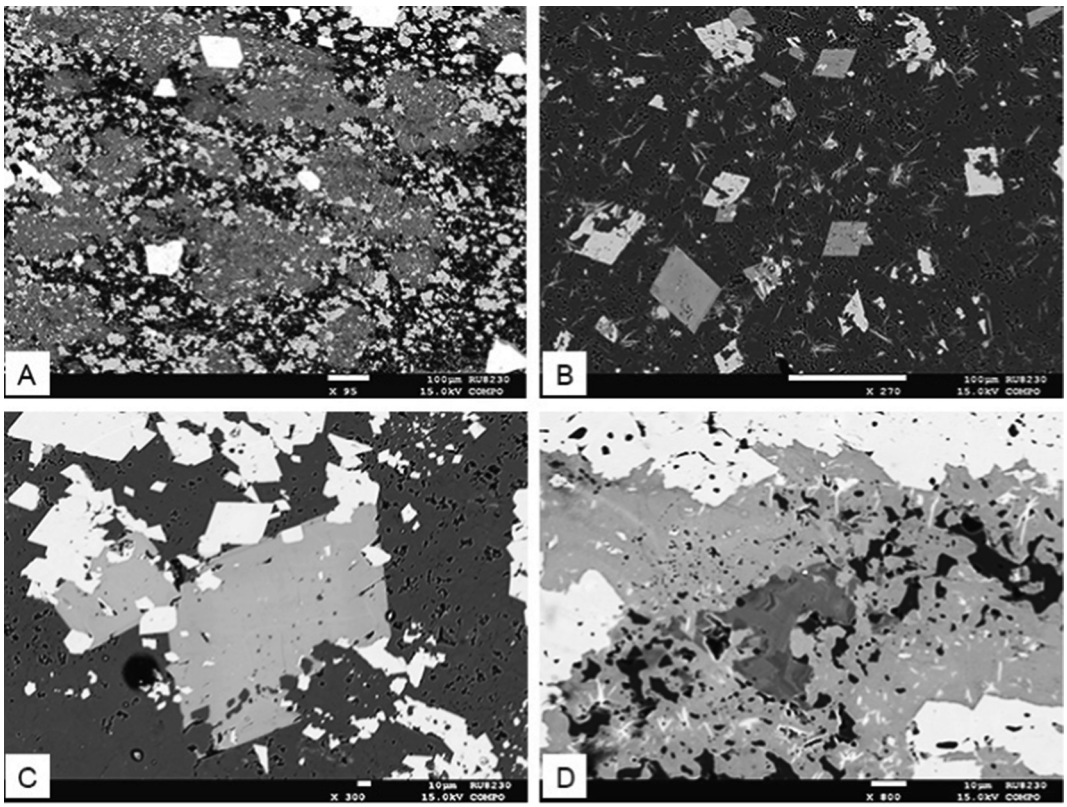

Fig. 5. Representative back-scattered electron (BSE) images of carbonate minerals from the Asbestos Hills IF. Image A illustrates first-order textural relationships between larger ankerite rhombohedra (darker grey) and coexisting brighter, finer-grained microsparitic disseminations of siderite scattered around the margins of the ankerite grains. Brightest grains represent magnetite. Image B displays coexisting siderite (light grey) and ankerite (grey) in fine microsparitic disseminations and occasional complex mutual intergrowths in a chert-minnesotaite matrix (dark background containing dispersed needles, respectively). Image C displays fine-scale textural relationships between larger euhedral ankerite (grey) with smaller siderite intergrowths along its grain edges (brighter grey). Dark background is chert. Image D illustrates relic HMC in the Kuruman IF replaced by darker subhedral aggregates of ankerite, succeeded by brighter siderite aggregates at the outer margin.

namely DIC at *circa* 0 ‰ and a fraction of the original biomass (TOC) at an assumed average value of about −28 ‰. Thompson et al (2019) further argue that the average $\delta^{13}C_{carb}$ of global IF at about −9 ‰ (Fig. 4) would reflect diagenetic mixing of the DIC and TOC reservoirs at an average DIC/TOC ratio of approximately 70:30. In a more nuanced extension of the same argument that takes into consideration the actual range of $\delta^{13}C_{carb}$ values shown in Fig. 4, the DIC/TOC ratio as sequestered and registered in IF would have ranged broadly between 80:20 and 50:50 at any given time during global iron formation deposition.

The interpretation of Thompson et al (2019) provides a simple means of addressing not only the lack of organic carbon preservation in IF but also the variability in the $\delta^{13}C_{carb}$ of IF carbonates (siderite, ankerite) through diagenetic mixing between isotopically heavy DIC and ^{13}C-depleted TOC. Thompson et al (2019) also posit that the shuttling of DIC-sourced carbon to precursor IF sediment would have been attained through primary, water-column siderite precipitation, ultimately mixing with isotopically light siderite in the sediment produced *via* anaerobic TOC diagenesis (*i.e.,* DIR). To this end, our new stratigraphic $\delta^{13}C_{carb}$ profiles combined with recently published results on the mineral chemistry of IF carbonates (Siahi et al, 2020) provide additional insights and constraints.

A key basis for our arguments that follow is the curiously homogeneous chemical composition of iron carbonate minerals that we have studied and reported from the Transvaal IF record (Siahi et al, 2020). Ankerite and siderite populations in our rocks, whether as monomineralic occurrences or as mixtures of the two species (Fig. 5), exhibit remarkable small-scale homogeneity in terms of their MgO/FeO and MnO/FeO abundance ratios. This chemical homogeneity when combined with the commonly euhedral textural habit of individual carbonate grains and aggregates (Fig. 5) suggests that any compositionally distinct populations of carbonate minerals representing potentially discrete carbonate sources are likely to have been erased during diagenetic carbonate transformations. In simple terms, we consider it impossible to physically distinguish different generations of iron carbonate minerals based on textural observations and mineral-chemical analyses, at least insofar as the rocks we have investigated here and through our recent studies are concerned (Siahi et al, 2020).

The difficulty in resolving the relative contributions of marine-*versus* diagenetically derived carbonate in the bulk carbonate fraction of IF samples, compounds the problem of determining with sufficient confidence the mineralogical nature of primary carbonate precipitation during deposition of IF. Thompson et al (2019) propose without supporting details that marine carbonate precipitation must have been primary siderite with a $\delta^{13}C$ value at around 0 ‰. Whereas water-column siderite formation has been argued before as part of IF depositional models (*e.g.*, Konhauser et al, 2005), the estimated relative contribution of marine siderite of well above 50% of the overall carbonate budget in IF (Thompson et al, 2019) is at odds with widely proposed diagenetic models of iron carbonate formation in IF (*e.g.*, Heimann et al, 2010; Posth et al, 2013), which propose an almost exclusive mode of siderite formation occurring below the sediment–water interface *via* DIR. Furthermore, primary siderite precipitation cannot readily account for the molar $CaCO_3$ and $MgCO_3$ recorded in the carbonate fraction of IF, at least in terms of the Ca. Calcium is presumably recycled into – and therefore reflected in – the abundant ankerite fraction

contained in many IF (Siahi et al, 2020). To this end, Heimann et al (2010) proposed that the modal $CaCO_3$ fraction in IF is likely to have been sourced from seawater during primary calcite deposition carrying a typically marine $\delta^{13}C$ signature (*i.e.,* near-0 ‰), which would ultimately have become incorporated into ankerite – and far less so in siderite – during sediment diagenesis and burial.

The recent study of Siahi et al (2020) on the carbonate mineralogy of the Transvaal IF, along with many earlier studies on carbonate minerals in other IF globally (*e.g.* Baur et al, 1985; Beukes and Klein, 1990; Kaufman et al, 1990; Tsikos et al, 2003), demonstrate with sufficient clarity that no discussion around the origin of IF can be based on the simplistic premise that the sole primary carbonate mineral in IF was siderite. The natural consequence of this conclusion is that determining the ultimate origin of the carbonate fraction of IF becomes an extremely challenging and nuanced objective. For example, it remains unresolved whether the primary carbonate species was calcite, siderite, variable mixtures of both, and/or any other carbonate phase that may not be preserved in the actual rocks. It is also hitherto not clear whether any two (or more) primary carbonate species may have formed simultaneously in the ambient water column, perhaps at different depths and under contrasting physico-chemical conditions. It is also unknown whether the depositional fluxes of each of these carbonate species were temporally constant or variable; whether any of these carbonates may have undergone partial dissolution and open-system recycling through, for example, open-system diagenetic dissolution under transiently low-pH conditions; and most crucially with respect to carbon isotopes, whether these carbonate minerals may have nucleated – partly or wholly – in equilibrium with a seawater parcel characterised by a low $\delta^{13}C$ signature (*e.g.* deep marine waters charged with oxidized CH_4 or hydrothermally sourced CO_2; see also Jiang and Tosca, 2019).

The above considerations paint a highly nuanced landscape with respect to primary carbonate precipitation during IF deposition, which is compounded further by the possibility that the postulated diagenetic carbonate fraction of IF was also highly variable through time and controlled by several overlapping processes and effects. For example, it remains equally uncertain whether the original biomass deposited in precursor IF sediment had an invariant isotopic composition or was temporally variable in response to fluctuating sources and fluxes of TOC at any given time. It is also unknown whether diagenetic carbonate formation during DIR was largely monomineralic in the form of isotopically light siderite or it may have also occurred as a mixed carbonate phase in the presence of additional cationic species in pore fluid [*e.g.,* Mg(II) or Ca(II)]. Finally, it remains unconstrained whether open-system diagenesis was conservative with respect to organic carbon sequestration and redox cycling, or upward loss of re-mineralised TOC as low-$\delta^{13}C$ DIC into benthic marine waters was possible, at least partially.

Our only direct proxy for the isotopic composition of preserved TOC in the Transvaal IF is based on the $\delta^{13}C_{TOC}$ values determined from the vanishingly small amounts of bulk organic carbon contained in the IF samples of drill core GASESA (Fig. 2A). We already alerted the reader in our "Results" section earlier to the fact that such small abundances of TOC and, by extension, the values and range of $\delta^{13}C_{TOC}$ obtained from them, must be treated with extreme caution. This concern stems from the likelihood that such low concentrations commonly represent refractory carbon from non-marine sources, possible occasional contamination during sample handling, and/or analytical artefacts produced during instrumental determination of $\delta^{13}C_{TOC}$ on extremely low TOC contents. In short, the isotopic composition of the infinitely low amounts of TOC in our samples and in IF in general, arguably confounds considerations on its sources and possible redox cycling during primary deposition and diagenesis, rather than offering a robust proxy for such processes.

The two binary diagrams of Fig. 6 can provide some constraints on possible controls on bulk $\delta^{13}C_{carb}$ variability during IF deposition. Firstly, the binary diagram linking the bulk $\delta^{13}C_{carb}$ value with the corresponding sum of carbonate-hosted cations for each sample (expressed as the wt% sum of the oxides of Ca, Fe, Mg and Mn; see Fig. 6A) represents a possible measure for the temporal variability in $\delta^{13}C_{carb}$ against variation in modal abundance of preserved carbonate. Assuming conservative, closed-system diagenesis with respect to (at least) carbon, the modal abundance of bulk carbonate in IF would faithfully reflect the mixing of DIC from the seawater-derived carbonate fraction, with recycled TOC as hosted in the carbonate mineral fraction that formed entirely below the sediment–water interface during anaerobic diagenesis (*i.e.*, DIR). The added assumption for a constant depositional flux of near-0 ‰ marine carbonate to the precursor IF sediment through time, would in fact translate the bulk $\delta^{13}C_{carb}$ value into a reliable record of the relative abundance of TOC in the initial sediment at any time (see also Konhauser et al, 2017).

The second binary diagram (Fig. 6B) displays the relationship between bulk $\delta^{13}C_{carb}$ and the carbonate-hosted CaO/FeO molar ratio. This diagram also has the potential to constrain bulk $\delta^{13}C_{carb}$ variability in IF in response to variable inputs of seawater *versus* diagenetically formed carbonate, based on the assumption that the molar calcite fraction in IF is exclusively of primary marine origin and has a $\delta^{13}C$ value very close to 0 ‰, while isotopically light

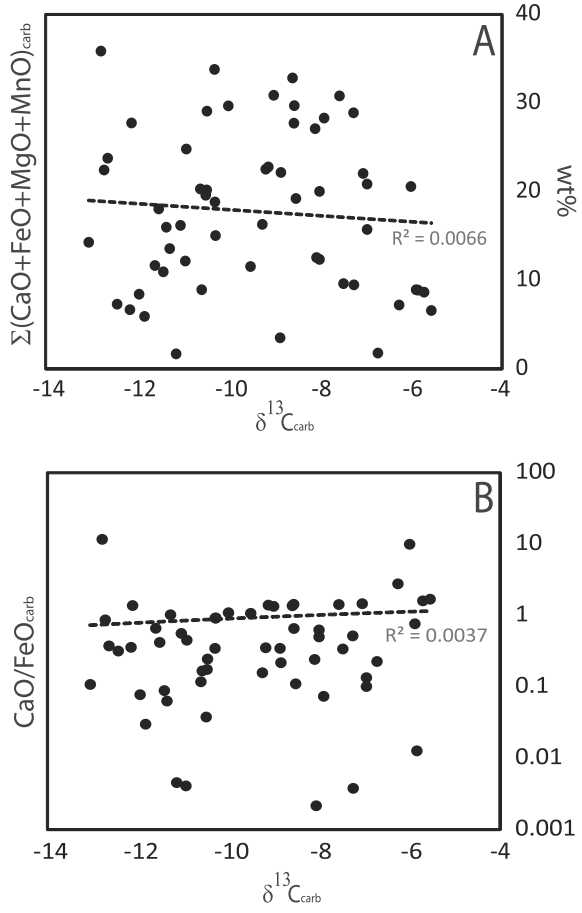

Fig. 6. Binary relationships against $\delta^{13}C_{carb}$ of drill core ERIN. A. Bulk modal carbonate expressed as the wt % total sum of carbonate-specific CaO, FeO, MgO and MnO data; B. CaO/FeO ratio of the carbonate fraction of each analysed sample.

iron carbonate would have formed exclusively *via* diagenetic DIR. Nevertheless, both diagrams of Fig. 6 show no relationship of statistical significance whatsoever and therefore fail to provide any meaningful constraints on bulk $\delta^{13}C_{carb}$ variability in IF through time. To the contrary, some additional questions emerge, such as the evidently well-constrained range in bulk $\delta^{13}C_{carb}$ of IF between −5 and −13 ‰ (Fig. 5), when the postulated range between end-member marine and diagenetic carbonate in IF is between 0 and −28 ‰. In simple terms, we consider puzzling why bulk $\delta^{13}C_{carb}$ values are not much lower than the value of-13 ‰ at least locally, for example in cases whereby diagenetic DIR may have transiently been the dominant contributing pathway to the bulk carbonate fraction of IF. Similarly, at least a few $\delta^{13}C_{carb}$ values higher than −5 ‰ would signify the occasionally overwhelming marine contribution to the bulk carbonate budget in IF, yet such values are rarely recorded in most IF.

The overarching conclusion derived from the above discussion, is that the laterally and vertically consistent carbonate $\delta^{13}C$ stratigraphy reported in this paper for the Asbestos Hills IF sequence of the Transvaal Supergroup, cannot be attributed with any certainty to a simple process of mixing of DIC *versus* organic carbon during deposition and diagenesis. It follows that the carbon isotope stratigraphy observed must either be regarded as *a priori* record of fluctuations in the DIC/TOC ratio of sequestered carbon in IF through time, or an alternative and hopefully more parsimonious interpretation would have to be sought. The following section exploits new evidence in support of such an alternative interpretation, followed by its possible first-order implications.

4.2. Primary carbonate deposition as the main control for $\delta^{13}C_{carb}$ variation in IF

Carbon isotope chemostratigraphy has been applied extensively to chemical sedimentary sequences of Phanerozoic age, emphasizing the $\delta^{13}C$ record of biogenic carbonate sediments and sedimentary rocks of unequivocal primary marine origin (*e.g.,* Jarvis et al, 2006). One of the common objectives of such applications is the elucidation of short-term perturbations in the global carbon cycle and their paleoenvironmental and paleoclimatic consequences (*e.g.,* Mesozoic Oceanic Anoxic Events; Tsikos et al, 2004). However, analogous applications targeting continuous IF sequences from the Precambrian sedimentary record have, to our knowledge, been comparatively neglected. A key reason for this gap appears to be the widely held contention that carbonate minerals in IF must be largely diagenetic in origin *via* microbially mediated processes of ferric iron reduction (DIR) and are therefore unlikely to have recorded primary seawater signals and processes in their stable isotope ratios (Fischer et al, 2009; Heimann et al, 2010; Johnson et al, 2013a).

One of the main arguments against exclusively primary, large-scale, low-$\delta^{13}C$ iron carbonate precipitation in Archaean ocean basins relates to the postulated requirement for much higher DIC concentrations in Archaean seawater compared to today. Elevated seawater DIC could, in turn, reflect exchange with an atmosphere characterised by correspondingly higher P_{CO2} levels than those at present, which are widely thought to have offset the climatic effects of lower solar luminosity in deep time (Kasting, 1993; Krissansen-Totton et al, 2018; Cattling and Zahle, 2020). Although precise constraints for atmospheric P_{CO2} before the GOE remain elusive, many authors also agree that a significant contribution of methane as additional greenhouse gas in the Archaean atmosphere would be warranted, at least periodically (Sheldon, 2006; Zerkle et al, 2012).

It follows that high DIC levels in Archaean seawater would have effectively dampened any isotopic effects and development of associated isotopic depth gradients related to organic carbon respiration in the oceanic water column, unless the biological carbon pump at that time was unrealistically stronger than it is today (Fischer et al, 2009). This of course does not mean that a biological pump was not operating during IF deposition, but rather that its isotopic effect in the ocean would have been effectively masked by a high ambient DIC content at near-0 ‰ $\delta^{13}C$. Any primary carbonate precipitation in equilibrium with Archaean seawater during the deposition of IF would thus be expected to record a $\delta^{13}C$ signature very similar to that of seawater DIC at that time (Fischer et al, 2009; Thompson et al, 2019).

Recent experimental studies, however, have revealed a new abiotic pathway of microsparitic iron carbonate precipitation, which is accompanied by strong kinetic isotopic effects on the fractionation of carbon isotopes (Jiang et al., 2022). The primary control for such fractionation is reported to be the degree of siderite supersaturation in ambient seawater, referred to as parameter "**Ω**" in Jiang et al (2022). Importantly, carbon isotope fractionation from an initial DIC pool of near-0 ‰ $\delta^{13}C$, appears to be large enough to account for the entire −13 to −5 ‰ range of $\delta^{13}C$ values typically recorded in IF carbonate minerals from the South African record and globally (Fig. 4).

Contrary to models involving DIR, we propose that primary iron carbonate formation and associated kinetic carbon isotope fractionation as detailed in the experimental work of Jiang et al (2022) provide a simple, feasible, and more parsimonious explanation for the development of vertically and laterally reproducible chemostratigraphic profiles for the carbonate $\delta^{13}C$ record of IF (Fig. 7). First-order variability in $\delta^{13}C_{carb}$ through time would be controlled by secular changes in water-column conditions of iron carbonate (super)saturation in response to ocean basin-wide fluctuations in key physicochemical parameters influencing carbonate formation, such as seawater alkalinity and pH (Thibon et al, 2019; Jiang et al, 2022). In essence, our interpretation removes the need to invoke unusually light DIC in the water column, while the regional consistency in $\delta^{13}C$ demands regional similarities in fractionations during carbonate precipitation. Additional inputs of low-$\delta^{13}C$ DIC involved in primary carbonate formation should also not be discounted, such as periodic contributions of hydrothermally sourced CO_2, isotopically light carbon from an active biological pump, and/or oxidation of methane (Fig. 7). In such cases, the $\delta^{13}C$ eventually recorded in the carbonate fraction of IF at any time, would reflect the cumulative fingerprint of any combination of the above processes and effects.

It ought to be stressed here that the experimental work of Jiang et al (2022) was focused entirely on the precipitation of primary end-member iron carbonate (siderite) from Fe(II)-rich solutions devoid of other cationic species such as Ca(II). It therefore does not provide a direct explanation for the widespread occurrence of low-$\delta^{13}C$ microsparitic ankerite which, as indicated earlier, is also a common and abundant component in the Asbestos Hills IF and in IF in general (see Fig. 5). Petrographic studies from the Asbestos Hills IF (Siahi et al, 2020) have reported the occasional preservation of Fe/Mn-bearing Mg calcite as an apparent precursor to ankerite and siderite growth through an interpreted process of bulk replacement. The textures observed by Siahi et al (2020) (see Fig. 5D of this study) may be regarded as broadly comparable to those observed by Jiang and Tosca (2019) attributed to amorphous iron carbonate (AFC) microspheres acting as apparent seeds for microsparitic siderite (over)growth. Close compositional [(Mg, Mn)O/FeO ratios] and isotopic ($\delta^{13}C$) similarities are also recorded in the Asbestos Hills IF between primary Mg calcite and the enveloping iron carbonates (Siahi et al, 2020); the isotopic similarities are further supported by the results of the sub-selection of six IF samples from this study for which separate ankerite and siderite fractions were targeted for $\delta^{13}C$ analyses (Al Aasm *et al,* 1991; see Fig. 2B). These observations collectively suggest that the

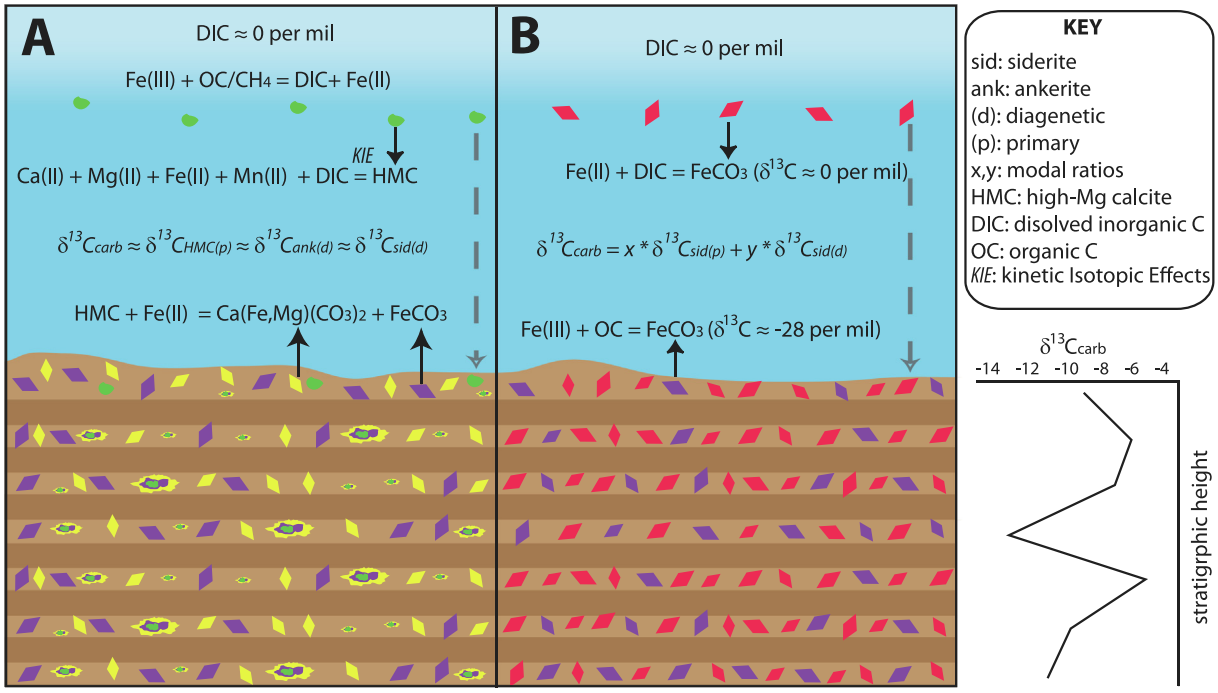

Fig. 7. Schematic illustration of two end-member pathways for low-$\delta^{13}C$ bulk carbonate formation in IF, leading to the reproducible inter-site carbon isotope chemostratigraphy recorded in the Asbestos Hills IF of the Transvaal Supergroup. A. Primary abiotic formation of low-$\delta^{13}C$, Fe/Mn-bearing HMC in an anoxic, high-DIC water column, followed by isotopically conservative overgrowth/replacement by ankerite and siderite (based on results by Siahi et al, 2020, and this study). The model assumes kinetic isotopic effects to carbonate formation (Jiang et al, 2022) but also makes allowance for the addition to the DIC pool of anaerobically respired, isotopically light carbon (TOC, CH_4) during an active biological pump. (B) Combination of primary siderite deposition in equilibrium with $\delta^{13}C_{DIC}$ at near-0 ‰, with diagenetic, low-$\delta^{13}C$ siderite formation following organic carbon remineralisation by primary ferric oxyhydroxides *via* DIR (Thompson et al, 2019). The hypothetical $\delta^{13}C_{carb}$ curve shown adjacent to the diagram is drawn in response to crudely depicted modal siderite relationships that would have been conservatively captured in primary IF sediment. Note that the model (B) based on the work of Thompson et al (2019), makes no provision for the occurrence of calcic carbonates in IF (calcite, ankerite), which are consequently not considered in the diagram. See text for detailed discussion.

experimental results of Jiang et al (2022) may find analogous application in chemically more complex aqueous environments of IF deposition, in which carbonate saturation may have reflected the presence of cationic species in addition to Fe(II) in seawater, such as Ca(II), Mg(II), and/or Mn(II). Future experimental studies involving combinations of the above cations in solution will likely shed further light on this issue.

5. Conclusions and implications

In this paper, we revisit the bulk carbon isotope composition of the carbonate fraction of IF as a possible proxy for primary carbonate formation in seawater during IF deposition. Our target sequence was the well-known Asbestos Hills Subgroup of the 2.6–2.2 Ga Transvaal Supergroup in the Northern Cape Province of South Africa (Griqualand West Basin). We obtained stratigraphically controlled, bulk $\delta^{13}C_{carb}$ data from five drillcore intersections capturing the largest stratigraphic portion of the Asbestos Hills IF and straddling a present geographical distance of over 25 km. Our approach was informed by an earlier study of ours (Siahi et al, 2020), in which we report evidence for preservation of apparently primary, low-$\delta^{13}C$ Mg calcite in the same rocks as a precursor to isotopically similar (with respect to carbon) ankerite and siderite.

We first assessed the consistently reproducible carbonate $\delta^{13}C$ stratigraphy of the Asbestos Hills IF strata against prevailing models of diagenetic formation of iron carbonates *via* DIR. We found no compelling petrographic or compositional (including isotopic) information in our rocks that would suggest with any certainty that the chemostratigraphic profiles presented here must reflect diagenesis *via* systematic, regionally uniform contributions to pore water DIC through TOC remineralization in the precursor IF sediment. We consequently argued that pathways of primary abiotic iron carbonate formation in the ancient water column accompanied by kinetic isotopic effects as recently explored by Jiang et al (2022) is likely to be the more plausible mechanism for the delivery of a qualitatively and quantitatively consistent, basin-wide stratigraphic trend in the low-$\delta^{13}C$ carbonate record of IF.

One of the obvious practical implications of our work is the potential utility of the carbon isotope record of IF as an effective stratigraphic correlation tool, at least within the geographical scales of a single paleobasin of widespread IF deposition. In the wider context of formation models for IF and their significance as key record of Earth's early biogeochemical evolution, our results encourage reassessment of current paleoenvironmental models for the early Earth and for the carbon cycle during IF deposition specifically. One of the common issues we recognise in recent competing models for IF genesis is that they tend to focus on the significance of specific Fe-rich mineral phases and their possible origins, overlooking the large compositional complexity of IF on wide-ranging scales of observation. For example, long-standing biogenic models for primary iron oxidation present ferrihydrite as essentially the sole mineral precursor to IF genesis, while the dominantly ferrous mineral character of IF is attributed mostly – if not exclusively – to a diagenetic environment of quantitative organic carbon respiration and coupled ferrihydrite reduction (Konhauser et al, 2005; Johnson et al, 2013a). In fact, only recently has the possibility of substantial primary iron carbonate formation in the water column from ambient Fe(II) received attention in efforts to account for the paucity of organic carbon preservation in IF (Thompson et al, 2019). In stark contrast, other emerging abi-

otic models for IF genesis in an anoxic, pre-GOE atmosphere–ocean system invoke the iron silicate mineral greenalite as the dominant precursor species in IF (Rasmussen et al, 2019, 2021), with the modally abundant magnetite attributed to secondary oxidation of Fe carbonate minerals (Rasmussen and Muhling, 2018). However, the possibility of a silicate precursor is offered without considering the clear compositional disparities between the silicate, oxide and carbonate fractions of IF, especially with respect to the mineralogical distribution of elements such as Mn (Oonk et al, 2017; Siahi et al, 2020).

We argue that effective modelling of the origin of IF should occupy the middle ground of the above two model extremes. Our stratigraphically controlled carbon isotope results in combination with the recent work of Jiang et al (2022) appear to lend further credence to entirely abiotic pathways of primary iron silicate and carbonate mineral formation in IF - that is, mechanisms that do not require Fe reduction *via* DIR. At the same time, the suggestion for abiotic magnetite formation *via* methanization of HCO_3^- or CO_3^{2-} in ferruginous waters by aqueous Fe(II) (Thibon et al, 2019) provides at least one alternative pathway for iron oxide formation in the absence of free molecular oxygen. It follows that the mineralogy, bulk redox state, and characteristic compositional banding of IF could result from entirely abiotic cyclic mechanisms of iron mineral precipitation in the absence of O_2, with profound implications for the role of IF in understanding biological and redox evolution models leading up to the GOE. At the centre of such abiotic pathways lies CO_2 and its aqueous speciation in seawater, as both an electron acceptor and control on seawater alkalinity and pH. Therefore, integral features of IF genesis such as the rhythmic microbanding and the variability in its isotopic record across time and space as displayed in the chemostratigraphic profiles of this study, may find explanations in temporal fluctuations in seawater alkalinity and pH during IF deposition rather than in the redox regime of the primary depositional and diagenetic environments.

We also assert that abiotic IF models need not preclude the possibility of at least transient biogenic contributions to primary ferric oxyhydroxide formation (*e.g.*, *via* photoferrotrophy or oxygenic photosynthesis) as an additional precursor contributor to the typical mineral assemblages of IF. Primary ferrihydrite formation, for example, may have operated at least, but its recycling in the water column by reduced carbon compounds may also have been possible and near-quantitative, thus accounting for the conspicuous absence of organic matter preservation in IF and the preponderance of magnetite as the chief oxide mineral. The isotopic effects of such an early biological pump in the pre-GOE ocean will likely remain difficult to unravel, as they may be obscured by the reportedly large kinetic isotopic effects accompanying iron carbonate supersaturation and attendant primary carbonate formation (Jiang et al, 2022). Irrespective of the above challenges, we are confident that our work opens new avenues of discovery for the broad topic of carbon cycling prior to the GOE, and particularly the multifaceted role of CO_2 during primary IF deposition.

CRediT authorship contribution statement

H. Tsikos: Conceptualization, Methodology, Supervision, Project administration, Funding acquisition, Writing – original draft. **M. Siahi:** Investigation, Formal analysis, Visualization. **S. Rafuza:** Investigation, Formal analysis, Visualization. **X.R. Mhlanga:** Investigation, Formal analysis, Visualization. **P.B.H. Oonk:** Investigation, Formal analysis, Visualization. **V. Papadopoulos:** Investigation, Formal analysis, Visualization. **A.J. Boyce:** Investigation, Validation. **P.R.D. Mason:** Investigation, Writing – review & editing. **C. Harris:** Investigation, Validation. **D.R. Gröcke:** Investigation, Validation. **T. W. Lyons:** Investigation, Writing – review & editing.

Declaration of Competing Interest

The authors declare that they have no known competing financial interests or personal relationships that could have appeared to influence the work reported in this paper.

Acknowledgements

H. Tsikos acknowledges generous funding by ASSMANG Ltd for the establishment of research unit PRIMOR while he was at Rhodes University in 2014-21. The company SOUTH32 in Hotazel, particularly Mr T. Rambuda and Mr E.P. Ferreira, are thanked for providing unconstrained access to all drill cores used in this study. D.R. Gröcke acknowledges SIBL for covering the organic carbon isotope analyses. T.W. Lyons and P.R.D. Mason acknowledge financial support from Rhodes University through the Hugh Kelly Visiting Fellowship for 2014 and 2016, respectively. The NSF-EAR FESD Program and the NASA Astrobiology Institute under Cooperative Agreement No. NNA15BB03A issued through the Science Mission Directorate Contributions provided support to Lyons.

References

Al-Aasm, I.S., Taylor, B.E., South, B., 1990. Stable isotope analysis of multiple carbonate samples using selective acid extraction. Chem. Geol. 80, 119–125.
Baur, M.E., Hayes, J.M., Studley, S.A., Walter, M.R., 1985. Millimeter-scale variations of stable isotope abundances in carbonates from Banded Iron Formations in the Hamersley Group of Western Australia. Econ. Geol. 80, 270–282.
Becker, R.H., Clayton, R.N., 1972. Carbon isotopic evidence for the origin of a Banded Iron-Formation in Western Australia. Geochim. Cosmochim. Acta 36, 577–595.
Beukes, N.J., Klein, C., 1990. Geochemistry and sedimentology of a facies transition — from microbanded to granular Iron-Formation — in the early Proterozoic Transvaal Supergroup, South Africa. Precambr. Res. 47, 99–139.
Catling, D.C., Zahnle, K.J., 2020. The Archean atmosphere. Sci. Adv. 6, eaax1420.
Crowe, S.A., Paris, G., Katsev, S., Jones, C., Kim, S.T., Zerkle, A.L., Nomosatryo, S., Fowle, D.A., Adkins, J.F., Sessions, A.L., Farquhar, J., Canfield, D.E., 2014. Sulfate was a trace constituent of Archean seawater. Science 346, 735–739.
Dodd, M.S., Papineau, D., Pirajno, F., Wan, Y., Karhu, J.A., 2019. Minimal biomass deposition in banded iron formations inferred from organic matter and clay relationships. Nat. Commun. 10, 1–13.
Fischer, W.W., Schroeder, S., Lacassie, J.P., Beukes, N.J., Goldberg, T., Strauss, H., Horstmann, U.E., Schrag, D.P., Knoll, A.H., 2009. Isotopic constraints on the Late Archean carbon cycle from the Transvaal Supergroup along the western margin of the Kaapvaal Craton, South Africa. Precambr. Res. 169, 15–27.
Fröelich, P.N., Klinkhammer, G.P., Bender, M.L., Luedtke, N.A., Heath, G.R., Cullen, D., Dauphin, P., Hammond, D., Hartman, B., Maynard, V., 1979. Early oxidation of organic matter in pelagic sediments of the eastern equatorial Atlantic: suboxic diagenesis. Geochim. Cosmochim. Acta 43, 1075–1090.
Heimann, A., Johnson, C.M., Beard, B.L., Valley, J.W., Roden, E.E., Spicuzza, M.J., Beukes, N.J., 2010. Fe, C, and O isotope compositions of banded iron formation carbonates demonstrate a major role for dissimilatory iron reduction in ~2.5 Ga marine environments. Earth Planet. Sci. Lett. 294, 8–18.
Jarvis, I., Gale, A.S., Jenkyns, H.C., Pearce, M.A., 2006. Secular variation in Late Cretaceous carbon isotopes: a new $\delta^{13}C$ carbonate reference curve for the Cenomanian-Campanian (99.6–70.6 Ma). Geol. Mag. 143, 561–608.
Jelavic, S., Mitchell, A.C., Sand, K.K., 2020. Fate of organic compounds during transformation of ferrihydrite in iron formations. Geochem. Persp. Lett. 15, 25–29.
Jiang, C.Z., Tosca, N.J., 2019. Fe(II)-carbonate precipitation kinetics and the chemistry of anoxic ferruginous seawater. Earth Planet. Sci. Lett. 506, 231–242.
Jiang, C.Z., Halevy, I., Tosca, N.J., 2022. Kinetic isotope effect in siderite growth: Implications for the origin of banded iron formation siderite. Geochim Cosmochim. Acta 322, 260–273.
Johnson, C.M., Ludois, J.M., Beard, B.L., Beukes, N.J., Heimann, A., 2013a. Iron formation carbonates: paleoceanographic proxy or recorder of microbial diagenesis? Geology 41, 1147–1150.
Johnson, J.E., Webb, S.M., Thomas, K., Ono, S., Kirschvink, J.L., Fischer, W.W., 2013b. Manganese-oxidizing photosynthesis before the rise of cyanobacteria. Proc. Natl. Acad. Sci. 110, 11238–11243.
Kasting, J.F., 1993. Earth's early atmosphere. Science 259, 920–925.
Kaufman, A.J., Hayes, J.M., Klein, C., 1990. Primary and diagenetic controls of isotopic compositions of iron-formation carbonates. Geochim. Cosmochim. Acta 54, 3461–3473.
Klein, C., Gole, M.J., 1981. Mineralogy and petrology of parts of the Marra Mamba iron formation, Hamersley Basin, Western Australia. Am. Mineral. 66, 507–525.
Klein, C., 2005. Some Precambrian banded iron-formations (BIFs) from around the world: Their age, geologic setting, mineralogy, metamorphism, geochemistry, and origin. Am. Mineral. 90, 1473–1499.

Konhauser, K.O., Newman, D.K., Kappler, A., 2005. The potential significance of microbial Fe(III) reduction during deposition of Precambrian banded iron formations. Geobiology 3, 167–177.
Konhauser, K.O., Planavsky, N.J., Hardisty, D.S., Robbins, L.J., Warchola, T.J., Haugaard, R., Lalonde, S.V., Partin, C.A., Oonk, P.B.H., Tsikos, H., Lyons, T.W., Bekker, A., Johnson, C.M., 2017. Iron formations: A global record of Neoarchaean to Palaeoproterozoic environmental history. Earth Sci. Rev. 172, 140–177.
Krissansen-Totton, J., Arney, G.N., Catling, D.C., 2018. Constraining the climate and ocean pH of the early Earth with a geological carbon cycle model. Proc. Natl. Acad. Sci. U.S.A. 115, 4105–4110.
Mhlanga, X.R., 2019. A reappraisal of the origin of the Hotazel iron-manganese Formation in an evolving early Earth system, through the application of mineral-specific geochemistry, speciation techniques and stable isotope systematics. Rhodes University, p. 161p. Unpublished PhD thesis.
Miyano, T., Klein, C., 1983. Conditions of riebeckite formation in the iron-formation of the Dales Gorge Member, Hamersley Group, Western Australia. Am. Mineral. 68, 517–529.
Nealson, K.H., Myers, C.R., 1990. Iron reduction by bacteria: a potential role in the genesis of banded iron formations. Am. J. Sci. 290, 35–45.
Oonk, P.B.H., Tsikos, H., Mason, P.R.D., Henkel, S., Staubwasser, M., Fryer, L., Poulton, S.W., Williams, H.M., 2017. Fraction-specific controls on the trace element distribution in iron formations: Implications for trace metal stable isotope proxies. Chem. Geol. 474, 17–32.
Posth, N.R., Köhler, I., Swanner, D.E., Schröder, C., Wellmann, E., Binder, B., Konhauser, K.O., Neumann, U., Berthold, C., Nowak, M., Kappler, A., 2013. Simulating Precambrian banded iron formation diagenesis. Chem. Geol. 362, 66–73.
Poulton, S.W., Canfield, D.E., 2005. Development of a sequential extraction procedure for iron: implications for iron partitioning in continentally derived particulates. Chem. Geol. 214, 209–221.
Rasmussen, B., Muhling, J.R., 2018. Making magnetite late again: Evidence for widespread magnetite growth by thermal decomposition of siderite in Hamersley banded iron formations. Precambr. Res. 306, 64–93.
Rasmussen, B., Muhling, J.R., Tosca, N.J., Tsikos, H., 2019. Evidence for anoxic shallow oceans at 2.45 Ga: Implications for the rise of oxygenic photosynthesis. Geology 47, 622–626.
Rasmussen, B., Muhling, J.R., Krapež, B., 2021. Greenalite and its role in the genesis of early Precambrian iron formations – A review. Earth Sci. Rev. 217, 103613.
Schneiderhahn, E.A., Gutzmer, J., Strauss, H., Mezger, K., Beukes, N.J., 2006. The chemo-stratigraphy of a Paleoproterozoic MnF- BIF succession – the Voëlwater Subgroup of the Transvaal Supergroup in Griqualand West, South Africa. S. Afr. J. Geol. 109, 63–80.
Sheldon, N.D., 2006. Precambrian paleosols and atmospheric CO_2 levels. Precambr. Res. 147, 148–155.
Siahi, M., Tsikos, H., Rafuza, S., Oonk, P.B.H., Mason, P.R.D., Mhlanga, X.R., van Niekerk, D., Harris, C., 2020. Insights into the processes and controls for the absolute abundance and distribution of manganese in Precambrian Iron Formations. Precambr. Res. 350, 105878.
Thibon, F., Blichert-Toft, J., Tsikos, H., Foden, J., Albalat, E., Albarede, F., 2019. Dynamics of oceanic iron prior to the great oxygenation event. Earth Planet. Sci. Lett. 506, 360–370.
Thompson, K.J., Kenward, P.A., Bauer, K.W., Warchola, T., Gauger, T., Martinez, R., Simister, R.L., Michiels, C.C., Llirós, M., Reinhard, C.T., Kappler, A., Konhauser, K. O., Crowe, S.A., 2019. Photoferrotrophy, deposition of banded iron formations, and methane production in Archean oceans. Sci. Adv. 5, eaav2869.
Tsikos, H., Beukes, N.J., Moore, J.M., Harris, C., 2003. Deposition, Diagenesis, and Secondary Enrichment of Metals in the Paleoproterozoic Hotazel Iron Formation, Kalahari Manganese Field, South Africa. Econ. Geol. 98, 1449–1462.
Tsikos, H., Jenkyns, H.C., Walsworth-Bell, B., Petrizzo, M.R., Forster, A., Kolonic, S., Erba, E., Premoli Silva, I., Baas, M., Wagner, T., Sinninghe Damsté, J.S., 2004. Carbon-isotope stratigraphy recorded by the Cenomanian-Turonian Oceanic Anoxic Event: correlation and implications based on three key localities. J. Geol. Soc. London 161, 711–719.
Walker, J.C.G., 1984. Suboxic diagenesis in banded iron formations. Nature 309, 340–342.
Zerkle, A.L., Claire, M.W., Domagal-Goldman, S.D., Farquhar, J., Poulton, S.W., 2012. A bistable organic-rich atmosphere on the Neoarchaean Earth. Nat. Geosci. 5, 359–363.